Figure 6.5-12 is an example for this expression, within the stated range of $\overline{\Delta N^2}/\ell$, for an earth-space propagation path through a turbulent region of height 5 km. Note that σ_θ^2 is directly proportional to path length and independent of operating frequency. Also, $\sigma\theta$ decreases with increasing eddy size, ℓ , while phase fluctuation σ_θ increases with increasing eddy size.

Estimates (CCIR-1986b, Rpt. 564-3) indicate that the short-term variations in the angle-of-arrival may be of the order of 0.02 degrees (0.37 milliradians) at 1 degree elevation. This is higher than the theory predicts (see Figure 6.5-12), but the effect does decrease rapidly with increasing elevation angle. Crane (1976) reports values of $\sigma\theta$ within the bounds of Figure 6.5-12 for 7 GHz measurements made at varying elevation angles with a 37 m diameter antenna.

Generally, for beamwidths greater than 0.01 degree and elevation angles above 10 degrees, the angle-of-arrival fluctuations are masked by other fluctuations.

6.5.5 Fading and Gain Degradation Design Information

6.5.5.1 Fade Distribution Function Estimation. The estimates of gain reduction and signal variance parameters, R and S^2, have been presented. These quantities may be incorporated into distribution functions which are of the form used in link design. They represent the long term average fade statistics due to clear air amplitude and angle-of-arrival fluctuations. The estimates of R and S^2 may be more closely matched to local and seasonal conditions if a local estimate of C_n^2 is available. A hypothetical low elevation angle fade distribution is presented in Figure 6.5-13. The abscissa is referenced to the signal level received in the absence of turbulence, i.e., including free space loss and gaseous absorption. The point at which the signal level is R dB is also the mean of the received signal; thus, one point on the fade distribution is established. The fade distribution for turbulence-induced fluctuations is assumed to be log-normal, with mean and median being

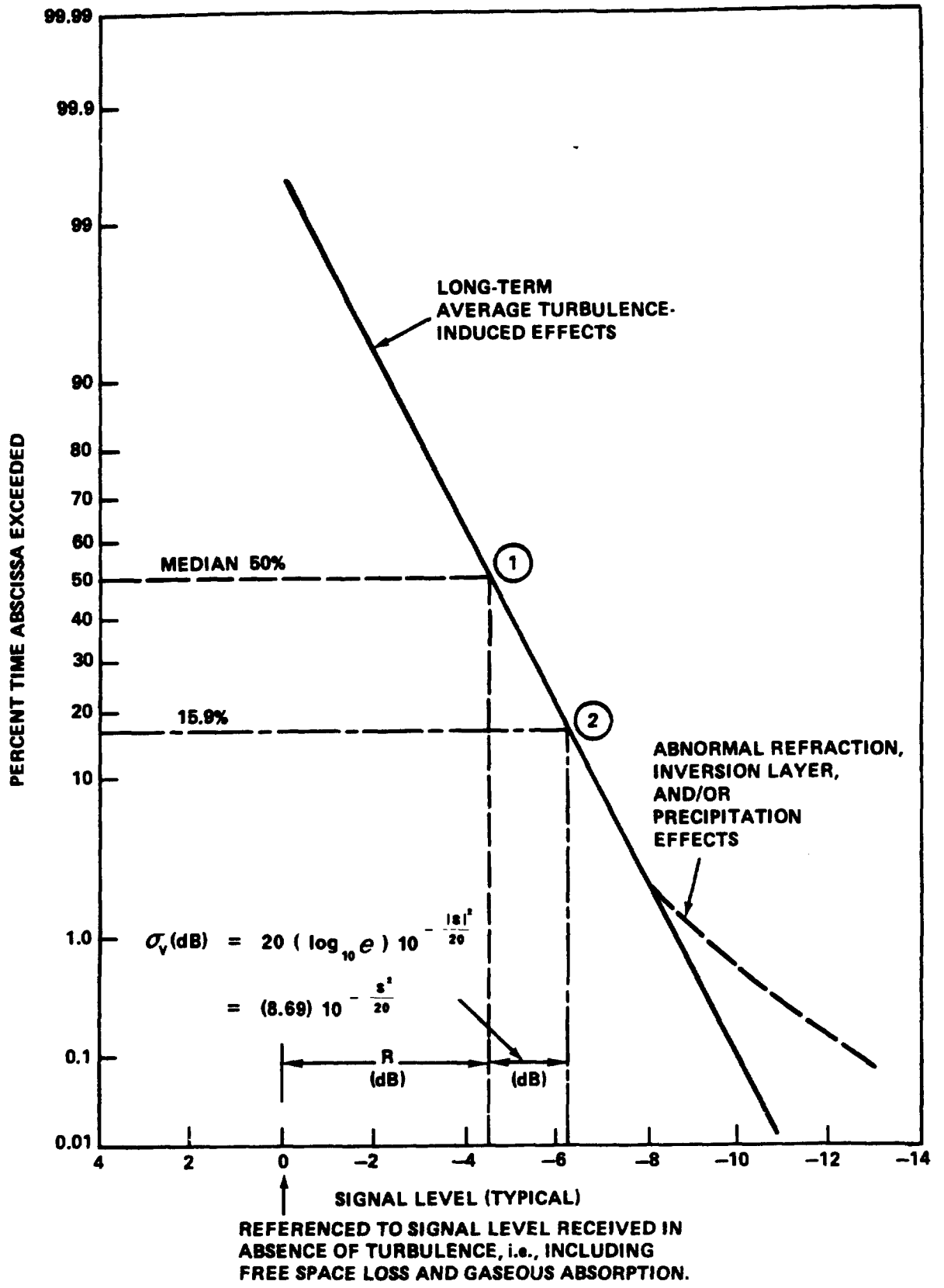

Figure 6.5-13. Hypothetical Fade Distribution Function for Low Elevation Angles

equal. The fade distributions resulting from the Ohio State University ATS-6 30 GHz beacon measurements (Devasirvatham and Hodge-1977) indicate that this log-normal assumption is valid for elevation angles above approximately 2°. A similar observation was made concerning the 7.3 GHz fade distribution above 4° elevation angle observed by McCormick and Maynard (1972).

A fade distribution may now be produced using this assumption of linearity. Referring to Figure 6.5-13, it was noted that the point at which the received signal level is R dB represents the mean signal level. For a normal distribution, the mean is plotted at the 50% time abscissa exceeded point, indicated by 1 in the figure. One standard deviation to the right of the mean on a normal distribution occurs at the 15.9% time abscissa exceeded level. It may be easily shown that the standard deviation of received signal level, expressed in dB and denoted $\sigma_{v_{dB}}$, may be written in terms of the signal variances S^2. This point, $\sigma_{v_{dB}}$, to the right of R, is denoted by 2 in the figure. A straight line drawn between points 1 and 2 now approximately represents the fade distribution, referenced to the mean signal level in the absence of turbulence induced fluctuations. This distribution was based on small fluctuation arguments and should be employed as a lower bound when estimating a particular fade distribution.

Deviation of this fade distribution from the expected form will occur at small time percentages. Additional fading due to precipitation, abnormal refraction, or inversions in the atmosphere will cause greater fade depths for the small time percentages. However, the turbulence effects, which are always present, are still dominant for larger time percentages. For high elevation angles, i.e., short path lengths, S^2 will be very small and the line drawn through points 1 and 2 will be virtually vertical.

However, the precipitation effects at the lower percentages will still be present for short path length cases and will become the dominant feature of the fade distribution.

6.5.5.2 Gain Degradation Design Information.

6.5.5.2.1 Estimation of Domains. The effects of amplitude and angle-of-arrival fluctuations are, of course, most prominent for very long path lengths and/or very narrow beamwidths. One may estimate whether or not gain degradation need be considered in a path design if elevation angle (or equivalent path length) and antenna beamwidth are known. Figure 6.5-14 presents regimes of average gain degradation between 0.5 and 3 dB and where they must be considered as a function of elevation angle and antenna beamwidth.

Realized gain, or expected gain less gain degradation, is plotted as a function of antenna beamwidth (for any frequency) or equivalent aperture diameter at 30 GHz in Figure 6.5-15. All equivalent aperture diameters are presented for an antenna aperture efficiency of 0.6. The curve representing zero path length L_t is simply the common gain approximation $G = 41253/B^2$ where B is the half power beamwidth in degrees. Realized gain curves for path lengths of 50 to 300 km are plotted using the model. Equivalent earth-space path elevation angles assuming a 6 km high homogeneous atmosphere are presented in parentheses.

Notice that gain degradation due to turbulence-induced fluctuation is negligible for beamwidths wider than about 0.7° for all path lengths. Degradation effects then gradually increase as beamwidth narrows from 0.7° to 0.05° and at any particular beamwidth are approximately directly proportional, in dB, to path length. As beamwidth narrows beyond 0.05°, a saturation effect occurs and the degradation becomes constant for any one path length.

All design figures of Section 6.5.5 represent estimates for clear air effects in a temperate climate during daytime and in the warmer months of the year. If a local value of C^2_n is known, more accurate values of R and S^2 may be obtained. If local statistics of C^2_n are known, statistics of R and S^2 may be obtained.

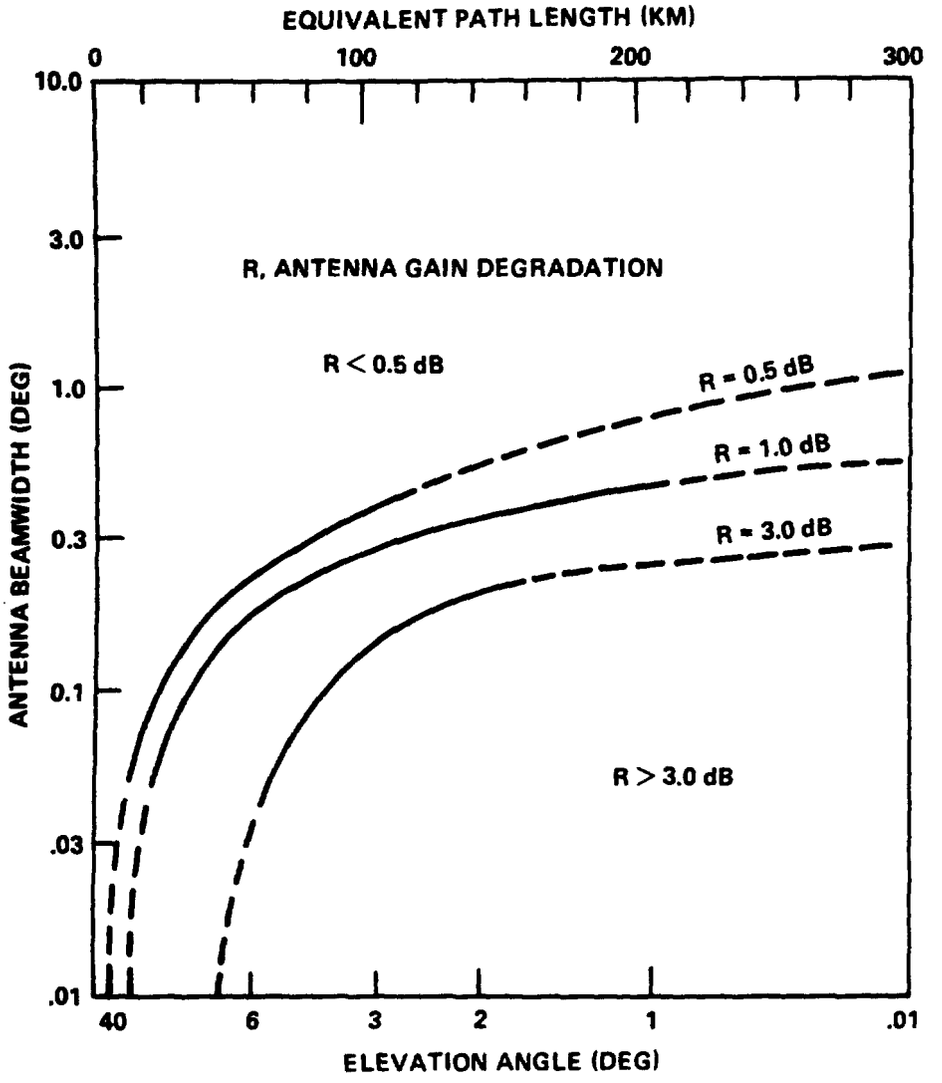

Figure 6.5-14. Gain Degradation Regimes as a Function of Beamwidth and Elevation Angle

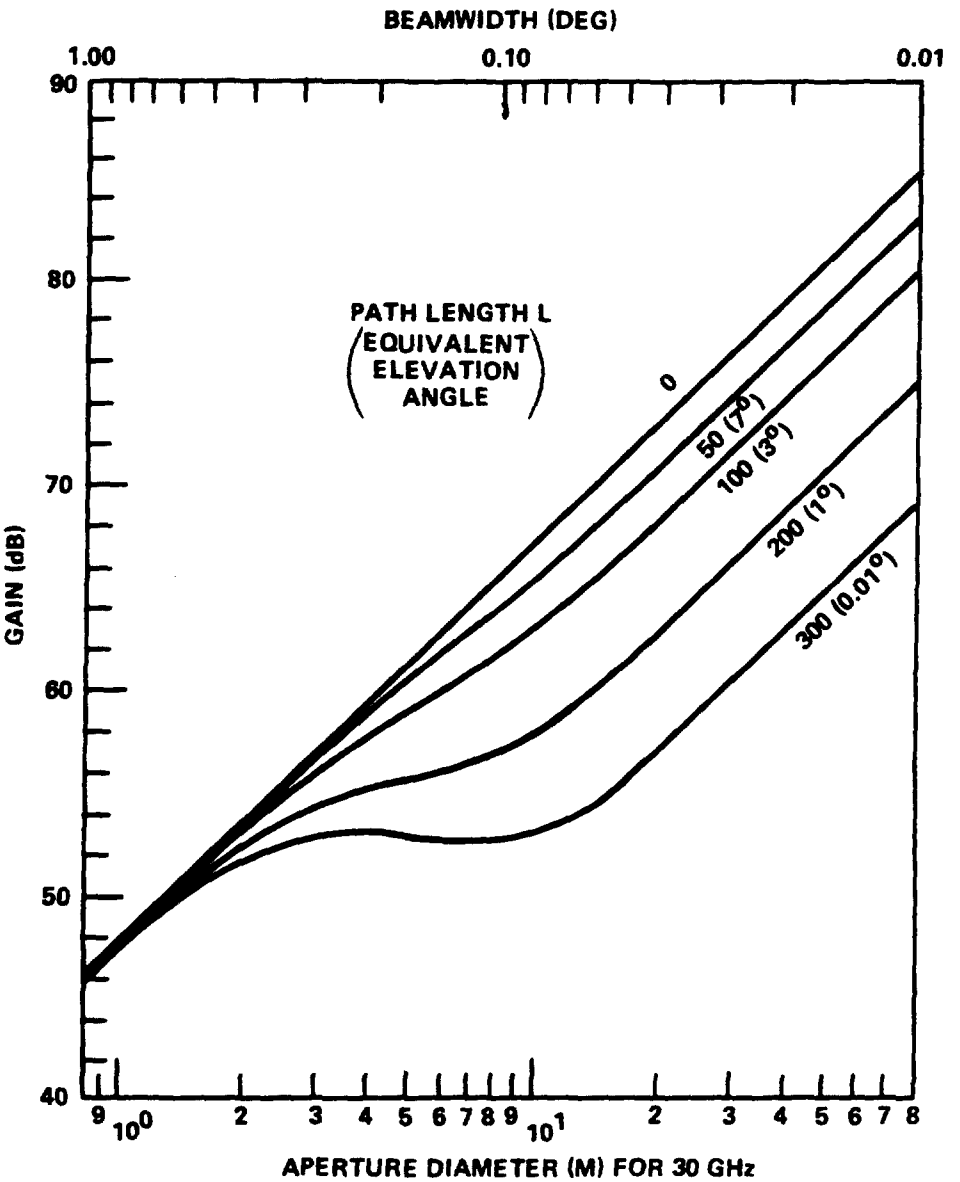

Figure 6.5-15. Realized Gain Versus Beamwidth or Aperture Diameter at 30 GHz

6.5.5.2.2 Spatial Diversity. Paths operating at very low elevation angles with narrow beamwidth antennas may experience unacceptable fading due to scintillation and multipath effects. The required reliability may be regained by the use of spaced site diversity. A site separation greater than 300 m transverse to the propagation path has been suggested (CCIR-1986b, Rpt 564-3) as necessary to alleviate severe turbulence-induced effects. In effect, separation on the order of or larger than the scale size of the largest inhomogeneities in refractive index along the propagation path, and especially near the surface where refraction is greatest, results in decorrelation of the instantaneous signal fluctuations and hence improved performance.

The aperture effects of large antennas may be circumvented if several phase-locked antennas, each with relatively wide beamwidth, are employed in an array to achieve the desired system gain. Of course, overall fade margins will be on the order of that for a single element, but angle-of-arrival effects are eliminated. In addition, such an array alleviates the need to mechanically track a geosynchronous satellite, as is necessary with large aperture, narrow beamwidth antennas.

6.5.6 A Sample Computation of Signal Fluctuations and Gain Degradation

In this section examples of the parameters described in Section 6.5 are worked out for a hypothetical ground station located at Columbus, Ohio with a 4.6m (15 ft) diameter parabolic antenna observing a 28.56 GHz COMSTAR beacon at 10 degrees elevation angle. Actually, the COMSTAR satellites are not at that low an angle, but in order to demonstrate the effects of gain reduction this value has been arbitrarily selected.

6.5.6.1 Amplitude Fluctuations. The variance of the received signal amplitude is calculated using the expression in Section 6.5.2.2. The full half-power beamwidth B in degrees is $70\lambda / d_a = 70 c/fd_a = (70)(3\times10^8 m/sec)/(28.56\times10^9 sec^{-1})(4.6m) = 0.16$ degrees. The

path length of the turbulence L_t is computed from h_t = 6 km, r_e = 6371 km and θ = 10 degrees using the equation

$$L_t = \left[h_t^2 + 2r_e h_t + (r_e \sin\theta)^2\right]^{1/2} - r_e \sin\theta = 34 \text{ km} \qquad (6.5\text{-}10)$$

The other constants are:

$$L_o = 180 \text{ km}$$

$$\delta^2_1 = 1.18 \times 10^{-3}$$

$$\delta^2_2 = 8.35 \times 10^{-4}$$

$$I_i = 0.17$$

$$I_c = 0.83$$

and the signal variance relative to the average power is

$$S^2 = 10 \log_{10} \frac{9.79 \times 10^{-4} + 0.14396 - 0.14297}{0.83 + 0.14}$$

$$= 10 \log_{10} (2.03 \times 10^{-3}) \simeq -27 \text{ dB}$$

Note that this agrees well with the results in Figure 6.5-2. Reference to Tatarski (1961) would have allowed evaluation in terms of C^2_n rather than the formulation by Theobold and Hodge (1978) utilized here.

Reference to Figure 6.5-4b indicates that 50% of the time the S^2 would be between -24 and -30 dB, while 90% of the time S^2 would be between -20 and -34 dB.

The power spectrum density of the fluctuations decreases at 26.5 dB/decade (see Figure 6.5-6). If one considers some lower frequency cutoff for the amplitude fluctuations (say 0.1 Hz) the

fluctuation power at 1 Hz is on the average 26.5 dB below the value of 0.1 Hz. Only 10% of the time will the 1 Hz fluctuation power be only 10 dB below the 0.1 Hz fluctuation power. Clearly, most of the fluctuation power for clear air fluctuations is at the low frequencies (less than 1 Hz).

6.5.6.2 Phase and Angle-Of-Arrival Variations. Phase fluctuations are estimated from the model of Muchmore and Wheelon (1955) presented in Section 6.5.3. Data quoted in Muchmore and Wheelon indicate typical values for $\ell \simeq$ 60m $\simeq$ 200 feet and $\overline{\Delta N^2} = 1/2$. Thus $\overline{\ell \Delta N^2} = 30$ meters.

For a finite circular antenna of 4.6 m diameter, the rms phase delay fluctuation is 0.85 radians = 48 degrees. For a $C_{no} = 10^{-14}$, the phase ripple fluctuation across the antenna is very small.

The estimate of the angle-of-arrival fluctuations in radians (see Section 6.5.4) is calculated to be 3.2×10^{-5} radians = 1.8×10^{-3} degrees. This is a small number compared to 0.16 degree half-power beamwidth of the antenna. Also note that the limits on $\Delta N^2/\ell = 8.3 \times 10^{-3} m^{-1}$ are not exceeded.

6.5.6.3 Prediction of the Average Received Signal Gain Reduction. The average received signal reduction is calculated using the same parameters required for calculation of the amplitude fluctuations. Using the relation in Section 6.5.2.2.4.

$$R = 10 \log_{10} \frac{(0.83 + 0.17(0.84))}{1.0} = -0.12 \text{ dB}$$

Thus during clear weather this COMSTAR beacon will on the average be 0.12 dB below the value calculated considering clear air attenuation only. This same value could be estimated from Figure 6.5-15.

The long-term average distribution in Figure 6.5-13 is now constructed from R and S^2. The point 2 (15.9% point) is found to be $20(\log_{10}e)\ 10^{-|S2|/20} = 0.39$ dB which is the standard deviation of the receiver voltage taken from a square law detector.

6.6 PREDICTION OF DEPOLARIZATION ON EARTH-SPACE PATHS

6.6.1 Introduction

Depolarization refers to that effect wherein an earth-space wave's polarization is altered in the troposphere. Depolarization is also referred to as cross-polarization. For linearly polarized waves a vertically (horizontally) polarized wave will, after passing through a medium, have a horizontally (vertically) polarized component in addition to the initial wave. For circularly polarized waves a RHCP (LHCP) wave will develop into an elliptical wave. For frequency reuse systems based on polarization isolation this coupling reduces isolation and increases "cross-talk."

6.6.1.1 **Sources of Depolarization.** The major source of depolarization at frequencies below 10 GHz is Faraday rotation of the plane of polarization by the Earth's ionosphere. Faraday rotation may be as much as 1° of rotation at 10 GHz. It is discussed in a companion publication of propagation effects at frequencies below 10GHz (Flock, 1987).

At frequencies above 10 GHz, the primary sources of depolarization are tropospheric and are due to the presence of

- hydrometeors (rain, ice, snow)
- multipath
- refractive effects

These hydrometeor and scattering effects generate depolarization because of the non-spherical shapes of the hydrometer particles. For example, as raindrop sizes increase their shape departs from spherical and becomes an oblate spheroid with an increasingly pronounced flat bottom. For large drop sizes a concave depression

develops (Pruppacher and Pitter-1971). Polarized microwave energy scattered from these particles can easily be converted into an orthogonal polarization.

6.6.1.2 Measures of Depolarization. The measurement of depolarization by propagation researchers usually has been done utilizing orthogonally-polarized feeds on a single antenna while observing singly-polarized satellite signals. This parameter is called the cross-polarization discrimination (XPD) or cross-polarization ratio (XPR) defined as (Bostian, et al-1977)

$$XPD = \frac{\text{power output from co-polarized port}}{\text{power output from cross-polarized port}}$$

$$= (XPR)^{-1}$$

For perfect transmitting and receiving antennas and a perfect medium this isolation could become infinite, but with practical components some leakage is always present. Definitions and sample calculations of depolarization terms have been well documented in a tutorial report by Stutzman (1977).

Unfortunately, the system designer desires the cross-polarization isolation (XPI) term defined as

XPI (dB) = co-polarized signal power (dB)

- cross-polarized signal power (dB) on the same channel

Fortunately, for most levels of attenuation observed, XPI $\simeq$ XPD = $(XPR)^{-1}$ (Watson and Arbabi-1973).

6.6.1.3 Depolarization Measurements. Most experimental depolarization data has been obtained from the 11.7 GHz right-hand circularly polarized Communications Technology Satellite (CTS) beacon, the 19.04 and 28.56 GHz linear polarized AT&T COMSTAR satellite beacons, and the 11.6 GHz circularly polarized SIRIO beacon.

6.6.2 Rain Depolarization

6.6.2.1 Depolarization Versus Attenuation Relations. Correlation of depolarization with rain rate has not been too successful because of the many parameters required for these calculations. However, experimentally and analytically (Nowland, et al-1977a) it has been observed that rain-induced depolarization can be related to total attenuation by the formula

$$XPD = \tilde{a} - \tilde{b} \log_{10}(A) \qquad (6.6\text{-}1)$$

where XPD is the cross-polarization discrimination in dB and A is the total attenuation in dB due to rain (not including the clear air attenuation). $\tilde{a}$ and $\tilde{b}$ are empirical constants.

6.6.2.1.1 CCIR Approximation. The CCIR (1986b, Rpt. 564-3) has developed analytical approximations for the empirical constants $\tilde{a}$ and $\tilde{b}$ which give reasonable agreement for the XPD with existing theory and available data. The relationships are,

$$\tilde{a} = 30 \log(f) - 10 \log_{10}[0.516 - 0.484 \cos(4\tau)] - 40 \log_{10}(\cos\theta) + 0.0052\sigma^2 \qquad (6.6\text{-}2)$$

and

$$\tilde{b} = 20 \quad \text{for } 8 \le f \le 15 \text{ GHz}$$
$$= 23 \quad \text{for } 15 < f \le 35 \text{ GHz} \qquad (6.6\text{-}3)$$

where:

f = frequency, in GHz

τ = polarization tilt angle with respect to the horizontal, in degrees (τ = 45° for circular polarization)

θ = path elevation angle, in degrees

σ = standard deviation of the raindrop canting angle, in degrees

The above relationships are valid over the ranges:

$$8 \leq f \leq 35 \text{ GHz}$$

$$\theta \leq 60^{\circ}$$

$$0^{\circ} \leq \tau \leq 90^{\circ}$$

Recommended values for the standard deviation σ are:

Percent of Time	σ
1.0%	0°
0.1%	5°
0.1%	10°
0.001%	15°

The above results do not include the effects of ice depolarization. A CCIR factor for ice induced XPD is discussed later in Section 6.6.3.3.

6.6.2.1.2 VPI & SU and Univ. of Texas Results. The Virginia Polytechnic Institute and State University (VPI&SU) have analyzed their CTS (11.7 GHz) and COMSTAR (16.04 and 28.56 GHz) beacon depolarization data in two manners. The first technique is to compare the measured cumulative XPD with the measured cumulative rain attenuation statistics. These results are termed the statistical depolarization results. The second technique pairs "instantaneous" (half-minute) intervals of data for both parameters and smooths the data to obtain $\tilde{a}$ and $\tilde{b}$.

The results of these two techniques for 11.7 GHz data both from VPI&SU and the University of Texas (C.W. Bostian, et al-1979) are shown in Figure 6.6-1. Clearly these results indicate a wide spread of values have been obtained to date even though they are averaged over an entire year. The attenuation has been truncated at 5 dB because of the effects of ice depolarization (see Section 6.6.3).

VPI&SU has also related the XPD to attenuation for each month of 1978 for which 5 dB or greater fades occurred. These $\tilde{a}$ and $\tilde{b}$ results are shown in Table 6.6-1 for the number of half-minute samples indicated. The R^2 term, a correlation cofficient, is a measure of the goodness of the fit. The wide variations noted are simalar to those observed by other investigators.

Additional data from the University of Texas at Austin (Vogel - 1979) incorporating exceedance values is presented in Figure 6.6-2. These curves show the 10%, 50% (median) and 90% expectation of exceeded isolation for each attenuation. For example at 5 dB (meaning 4 dB $\leq$ A $\leq$ 5 dB) the XPD exceeded 23 dB for 90%, exceeded 28 dB for 50% and exceeded 33 dB for 10% of the data. The logarithmic fit to these three curves is

$$10\% : XPD - 42.9 - 17.5 \log_{10}A$$
$$50\% : XPD - 35.8 - 13.4 \log_{10}A$$
$$90\% : XPD - 31.5 - 12.6 \log_{10}A$$

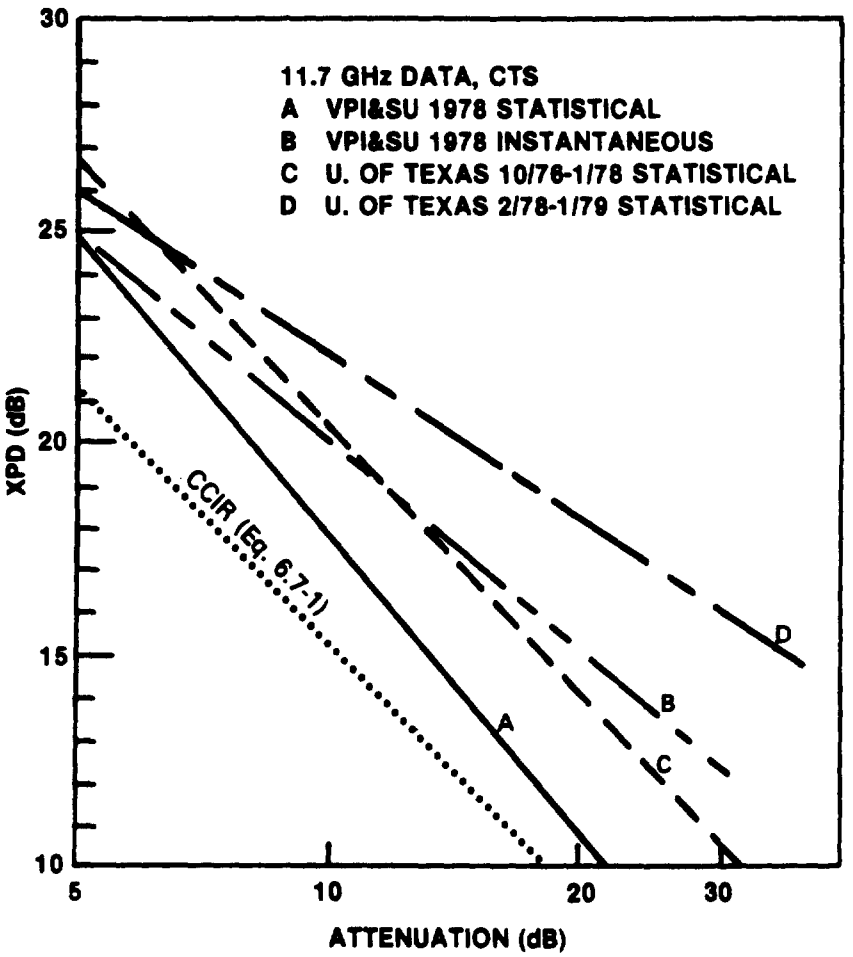

Figure 6.6-1. Cross-Polarization Discrimination Versus Attenuation for Statistical and Instantaneous Data

Table 6.6-1. Least-Mean Square Fits of Depolarization Coefficients by Month

$XPD = \tilde{a} - \tilde{b} \log_{10} A$ $\quad 5 < A < 30$ dB $\quad$ VPI&SU 1978 CTS DATA

MONTH	$\tilde{a}$	$\tilde{b}$	R^2	NO. OF 1/2 MINUTE INTERVALS
JAN	30.79	2.62	.00	22
MAR	51.18	38.18	.63	309
MAY	49.01	27.93	.90	30
JUNE	38.42	17.53	.56	38
JULY	42.23	21.94	.80	74
AUG	47.31	25.99	.47	28
SEPT	64.20	51.93	.32	50
NOV	27.59	4.11	.04	7
YEAR	36.29	16.22	.36	574

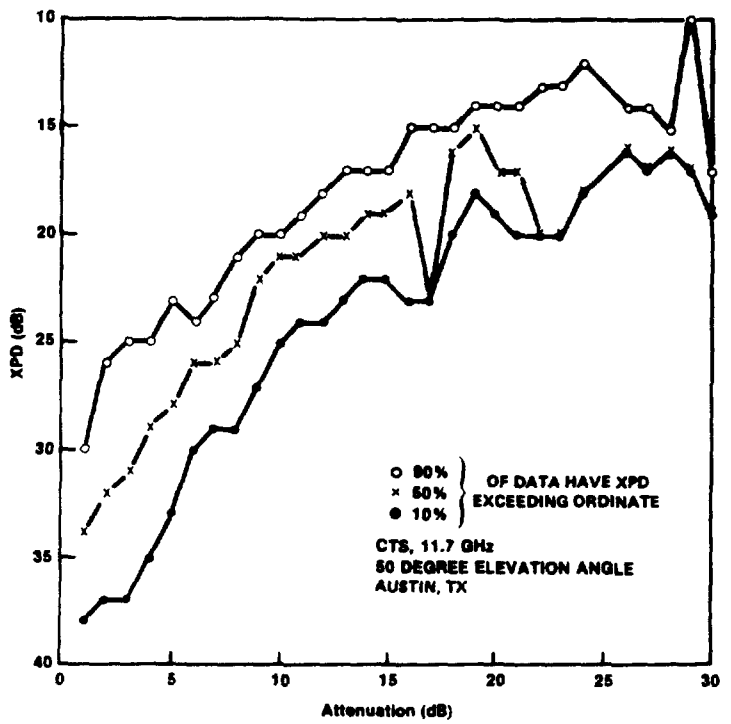

Figure 6.6-2. Twelve Month Isolation Versus Attenuation Data

for the 11.7 GHz CTS beacon at 50 degrees elevation angle.

6.6.2.2 Frequency Scaling Depolarization Measurements. The Virginia Polytechnic Institute and State University (Bostian, et al-1978, 1979) has also made simultaneous measurements of the depolarization at 19 GHz vertical and horizontal and 28.56 GHz using the COMSTAR beacons. Their results for 1977 and 1978 are given in Table 6.6-2.

Table 6.6-2. Cross-Polarization Discrimination Versus Attenuation (Least-Mean-Square Fits)

Blacksburg, VA		Elevation Angle = θ
Period	Frequency/Polarization	$XPD = \tilde{a} - \tilde{b} \log_{10}(A)$
Aug 1977	11 GHz, RHCP (CTS, $\theta = 33^{o}$)	$XPD = 44.7 - 22.6 \log_{10}(A)$
1978	11 GHz, RHCP (CTS)	$XPD = 36.3 - 16.2 \log_{10}(A)$
Aug 1977	19 GHz, vertical (COMSTAR, $\theta = 44^{o}$)	$XPD = 47 - 24.5 \log_{10}(A)$
Sept 1977	19 GHz, horizontal (COMSTAR)	$XPD = 37.1 - 20.0 \log_{10}(A)$
1978	19 GHz, vertical (COMSTAR)	$XPD = 43.9 - 16.6 \log_{10}(A)$
Aug 1977	28 GHz, vertical (COMSTAR)	$XPD = 36.4 - 15.4 \log_{10}(A)$
1978	28 GHz, vertical (COMSTAR)	$XPD = 31.2 - 7 \log_{10}(A)$

The analysis of Nowland, et al (1977a) may be utilized to show the expected frequency dependence of the coefficients $\tilde{a}$ and $\tilde{b}$ in $XPD = \tilde{a} - \tilde{b} \log_{10}(A)$. Using Equations 11 and 12 of Nowland, et al (1977a) and many of the constants in the paper, the solid curve was derived in Figure 6.6-3. The dashed curve was derived using the effective path length $L_e = 12.82\ R^{-0.3}$ and the specific attenuation in Section 6.3. Several experimental data points are shown, but

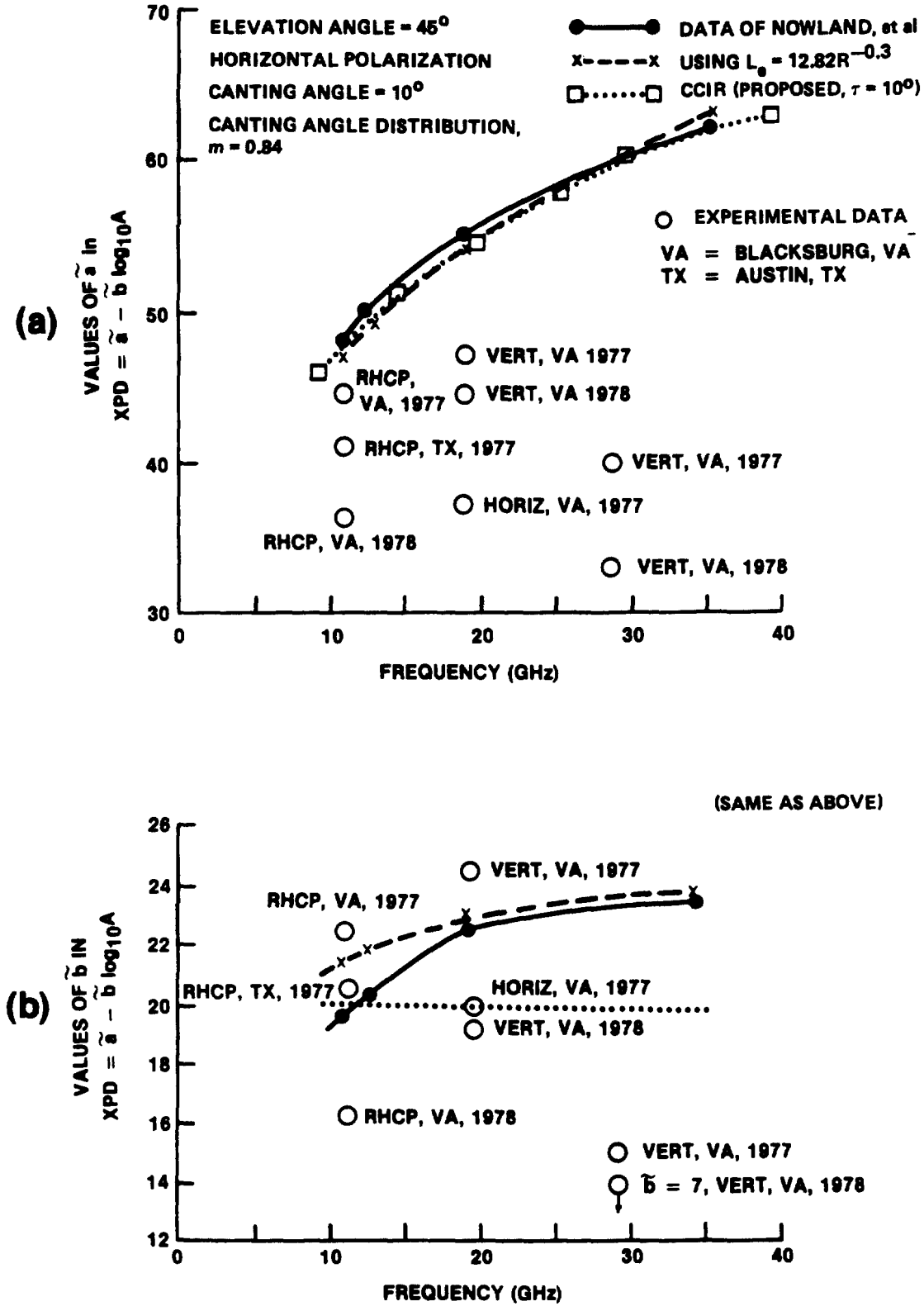

Figure 6.6-3. Frequency Dependence of the Coefficients in the Cross-Polarization Discrimination Relation

these do not correlate well with the theory (possibly because of the polarization dependence of $\tilde{a}$). The important results of these figures are that $\tilde{a}$ increases with increasing frequency, while $\tilde{b}$ appears to be relatively constant. In the relation $XPD = \tilde{a} - \tilde{b} \log_{10}(A)$ this would imply that the XPD increases with increasing frequency, but because of the rapid increase in A with frequency, XPD will actually decrease for increasing frequency and moderate rain rates.

Chu (1980) has found linear relations between the XPD and frequency throughout the 10 to 30 GHz frequency range. Specifically, XPD (expressed as a numerical ratio) is directly proportional to frequency for a fixed rain rate, and is inversely proportional to frequency for a fixed value of rain attenuation. Bostian (1979b) confirms this linear relation between the XPD (f_1) and XPD(f_2) from his monthly COMSTAR data for 1978, but, the value XPD(f_2)/XPD(f_1) varies from month to month.

6.6.2.3 Elevation Angle Dependence of Depolarization. In the U.S. and Canada depolarization measurements have been obtained at elevation angles from 10.7° in Blacksburg, VA (Bostian, et al-1986) to 49° at Austin, Texas (Vogel-1978). The general dependence of XPD versus A on elevation angle θ can be obtained from the theoretical results of Nowland, et al (1977a). Note that both the coefficient a and the total attenuation A depend on elevation angle.

The elevation angle dependent results of Nowland, et al (1977b) 11.7 GHz (experimental data) are shown in Figure 6.6-4. Clearly the a coefficient is elevation angle dependent, however the experimental data does not confirm this fact. The b coefficient appears to be nearly independent of elevation angle and does appear to agree with the limited data base.

Chu (1980) has observed that the differential propagation constant for depolarization is governed by a $\cos^2\theta$ relation.

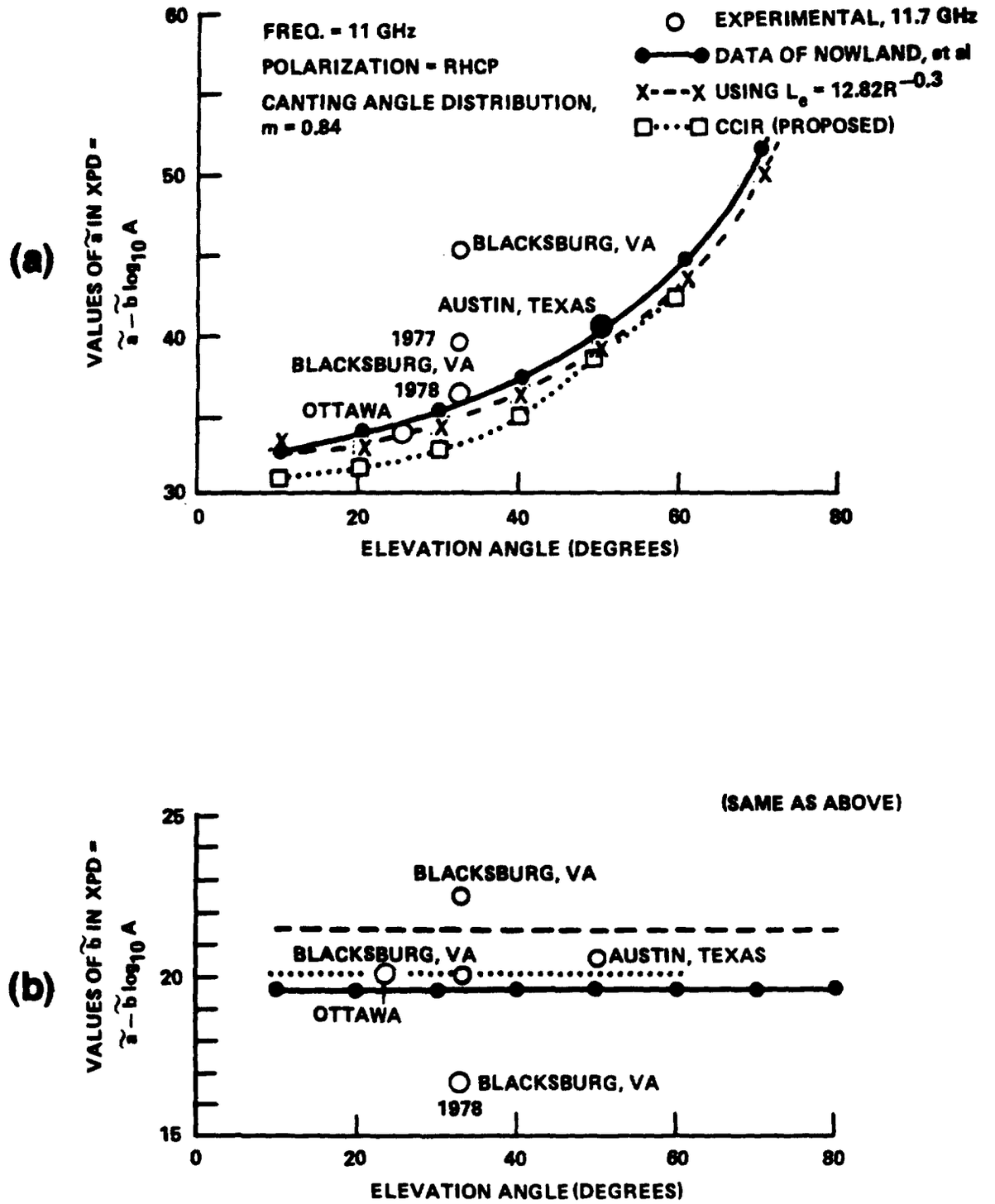

Figure 6.6-4. Elevation Angle Dependence of the Coefficients in the Cross-Polarization Discrimination Relation

However the XPD dependence on elevation angle must also take the effective path length effect into account (Chu-1974).

6.6.2.4 Phase Variations During Rain-Induced Depolarization Events. At Blacksburg, VA (Bostian, et al-1977) measurements have been made of the phase difference between the co-polarized signal components. This phase difference has been observed to both decrease and increase by about 150 degrees for 3 dB fades and then not change significantly for higher attenuations: The phase difference has also been observed to increase and then decrease in the same storm. The mechanism for this plateau at 150 degrees and why the sign changes remains unexplained.

6.6.3 Ice-Crystal Depolarization

6.6.3.1 Meteorological Presence of Ice. Ice crystals form around dust particles in shapes influenced by the ambient temperature. In cirrus clouds they may exist for an indefinite time, but in cumulonimbus clouds they follow a cycle of growth by sublimation, falling and melting in the lower reaches of the cloud (Bostian and Allnutt-1971b). Radio, radar and optical observations all confirm that cloud ice crystals possess some degree of preferred orientation related to the orientation of the electrostatic field. The crystals range in size from 0.1 to 1 mm and concentrations range from 10^3 to 10^6 crystals/m^3. The variation in concentration and occurrence of events may be due to the variation of "seed" nuclei in various air masses. For example continental air masses contain more dust nuclei than maritime air masses and so occurrences of ice-crystal depolarization occur more frequently at inland ground stations. This general trend has been observed between observations at the Virginia Polytechnic Institute and State University (inland, most frequent), University of Texas at Austin (intermediate) and Bell Telephone Laboratories (maritime, least frequent).

6.6.3.2 Ice-Crystal Depolarization Measurements. Ice particles well above the height of the melting layer may have significant cross-polarization effects even for small values of attenuation

(typically below 3 to 5 dB at 11.7 GHz). This effect is believed to contribute to the poor correlation between the excess attenuation and the cross-polarization discrimination at these low values of attenuation.

In Austin, TX (Vogel-1978, 1979) ice depolarization was associated with either thunderstorms during the summer months or with clouds in the presence of polar air masses during the winter. An example of the percentage of time that XPD was less than or equal to the abscissa given that the excess attenuation was less than or equal to 1 dB is shown for the 18 month period from 12 June 1976 to 31 January 1978 and the period February 1978 to January 1979 in Figure 6.6-5. This curve shows that during 1976-78 45 per cent of the time that the XPD was less than or equal to 35 dB, there was less than 1 dB of attenuation; 24 per cent of the time that the XPD = 30 dB the A = 1 dB and 12 per cent of the time that XPD = 25 dB the A ; 1 dB. In contrast, using the rain depolarization relation for 1 dB yields XPD = 40 dB. Therefore systems requiring 30 dB or more XPD should expect a significant number of depolarization events due to ice.

Also, it has been observed (Shutie, et al-1978) that at 30 GHz ice crystals yield a constant value (typically 90 degrees) of the relative phase angle between the crosspolar and copolar signals as a function of XPD as shown in Figure 6.6-6. The corresponding polar plot for a heavy rain event is shown in Figure 6.6-7. In this case the XPD was reduced by signal attenuation and the signal to noise ratio of the relative phase measurement decreased as the XPD decreased. This effect appears to increase the scatter of the phase angle with decrease in XPD.

English investigators have also noted that rapid changes in relative phase and XPD are observed in thunderstorms and are associated with realignment of the ice crystal orientation by the electrostatic fields. In electrically-active storms, these

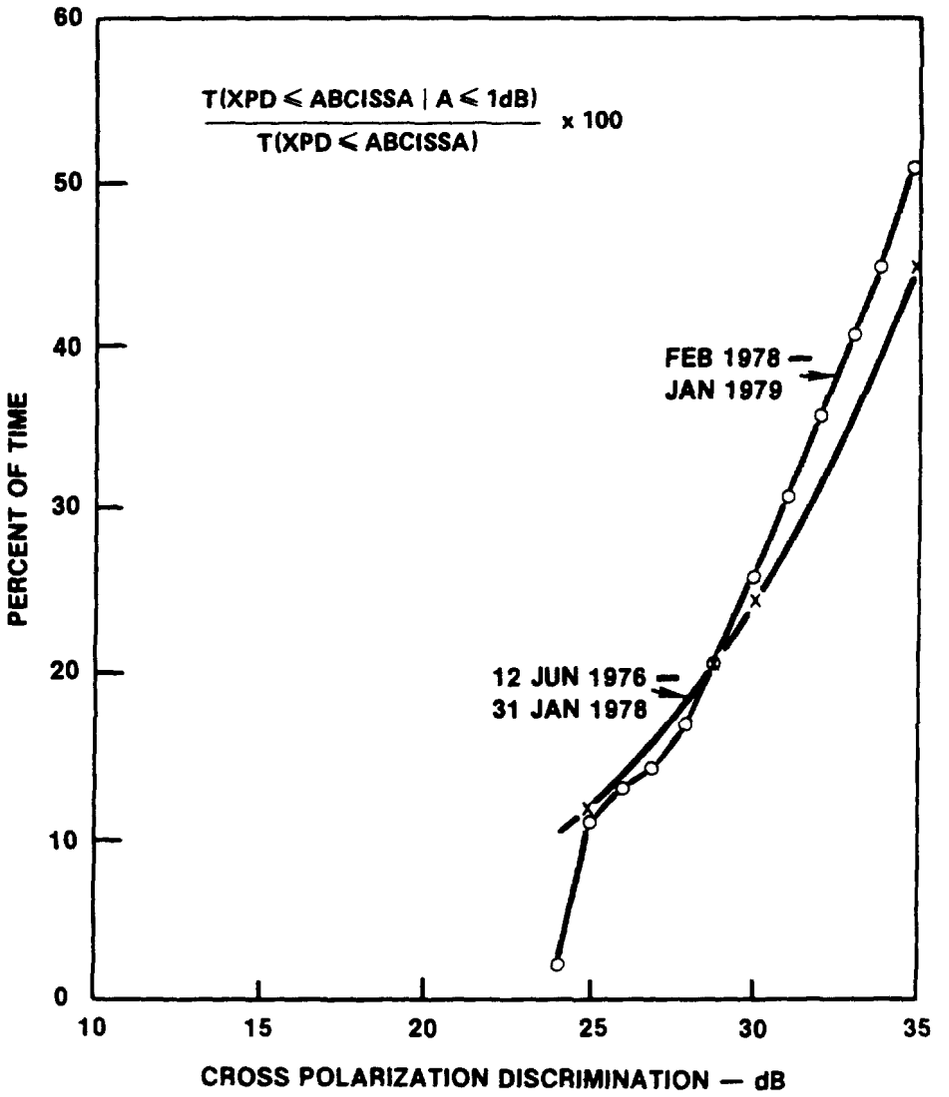

Figure 6.6-5. Contribution of Ice Depolarization to all Depolarization Events

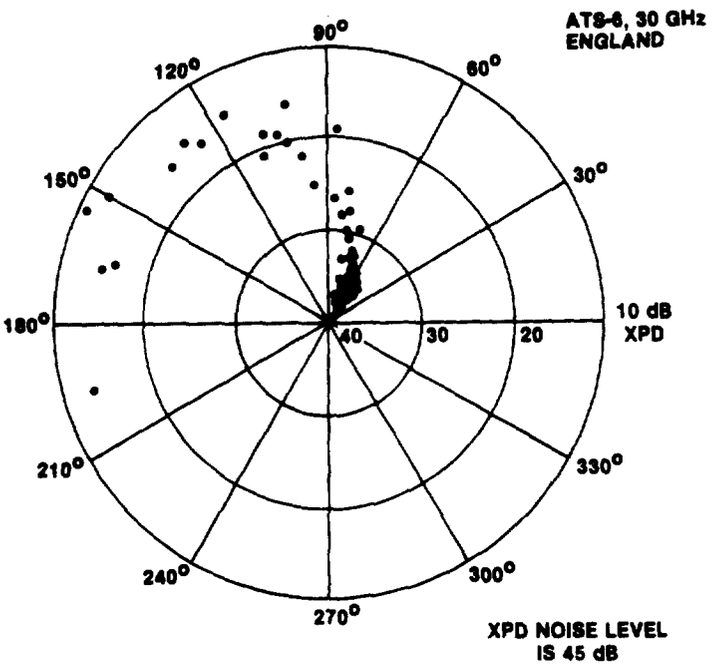

Figure 6.6-6. Polar Plot of the Cross Polarization Discrimination Arising from an Ice Cloud

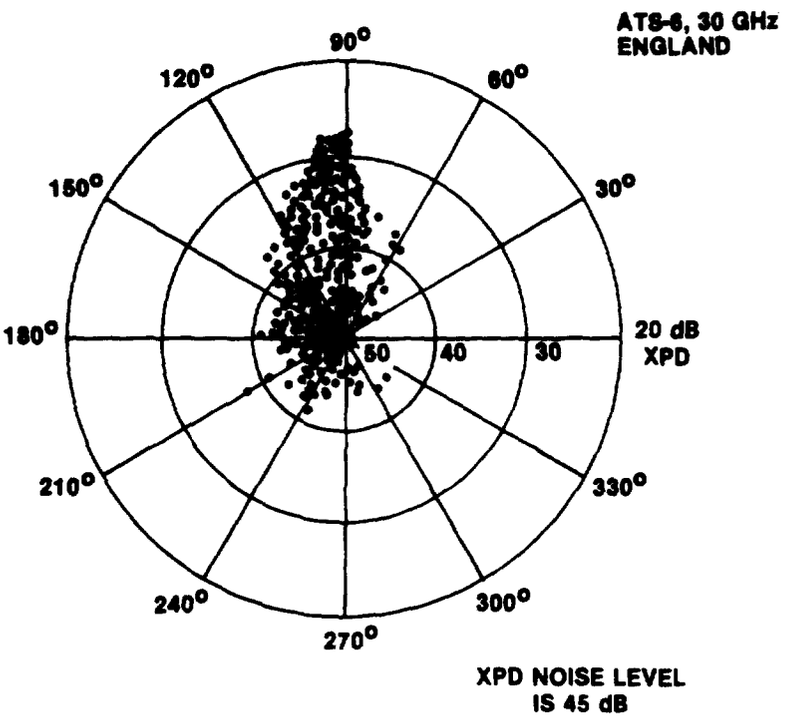

Figure 6.6-7. Polar Plot of the Cross Polarization Discrimination Arising from a Heavy Rain Event

electrostatic fields discharge rapidly resulting in rapid relative phase shifts of 180°, and rapid decreases in XPD of 27 dB in 20 seconds (Shutie, et al-1977) have been observed at the occurrence of a lightning flash. An example of this is shown in Figure 6.6-8 where the spikes in the relative phase occur for increasing XPD and result in large phase changes.

The spectra of rain and ice-induced crosspolarized signals have been analyzed (Hayworth, et al-1977) and it appears that a cancellation system with a 10 Hz bandwidth would track the majority of depolarizing events. However this bandwidth is probably insufficient during the sudden realignment of ice crystals in thunderstorms and in nonelectrically active precipitation. A suggestion has been made to consider use of a dual time constant system to accommodate all likely events.

For ice crystal depolarization the crosspolar phase shift is usually ±90 degrees of the copolarized signal and so differential attenuation dominates the XPD variations. This effect was displayed in Figure 6.6-6. However depending on the frequency, rain-induced XPD variations predominantly shift the phase near 20 GHz and below and induce differential attenuation from 20 to 60 GHz (Hogg and Chu-1975).

6.6.3.3 CCIR Estimation for Ice Depolarization. The CCIR (1986b, Rpt. 564-3) has provided an empirical factor, $C_{ice}(p)$, for estimating the contribution of ice deplarization at the percent of time p in terms of $XPD_{rain}(p)$, the cross polarization caused by rain. The resulting rain + ice XPD at the percent of time p, $XPD_T(p)$, is then determined from:

$$XPD_T(p) = XPD_{rain}(p) - C_{ice}(p) \quad \text{, in dB} \qquad (6.6\text{-}4)$$

where,

$$C_{ice}(p) = \frac{0.3 + 0.1\log_{10} p}{2} XPD_{rain}(p) \qquad (6.6\text{-}5)$$